Desalination and Water Treatment
www.deswater.com
doi: 10.1080/19443994.2014.960462

56 (2015) 2382–2394
November

Taylor & Francis
Taylor & Francis Group

Graphene oxide nanosheet: preparation and dye removal from binary system colored wastewater

Zahra Hosseinabadi-Farahani[a], Hassan Hosseini-Monfared[a], Niyaz Mohammad Mahmoodi[b,*]

[a]*Faculty of Science, Department of Chemistry, University of Zanjan, Zanjan, Iran, Tel. +98 241 5152576; Fax: +98 241 2283203; emails: zahrahof_80@yahoo.com (Z. Hosseinabadi-Farahani), monfared@znu.ac.ir (H. Hosseini-Monfared)*
[b]*Department of Environmental Research, Institute for Color Science and Technology, Tehran, Iran, Tel. +98 021 22969771; Fax: +98 021 22947537; emails: mahmoodi@icrc.ac.ir, nm_mahmoodi@aut.ac.ir, nm_mahmoodi@yahoo.com (N.M. Mahmoodi)*

Received 12 March 2014; Accepted 26 August 2014

ABSTRACT

In this paper, graphene oxide (GO) was prepared from graphite and used as an adsorbent to remove cationic dyes from single and binary systems of colored wastewater. The GO was prepared by Hummer method and characterized using Fourier transform infrared, scanning electron microscopy, and X-ray diffraction. Basic blue 41 (BB41), basic red 18 (BR18), and basic red 46 (BR46) were used as model dyes. It was found that the adsorption of dyes on GO followed the Langmuir isotherm and the pseudo-second-order kinetics. The capacity of GO to remove BB41, BR18, and BR46 was 1429, 1250, and 476 mg/g, respectively. The results show that the GO has a good capacity for dye adsorption from single and binary systems of colored wastewater containing cationic dyes.

Keywords: Preparation; Graphene oxide nanosheet; Dye removal; Binary system; Wastewater

1. Introduction

A variety of organic dyes are used in different industries such as textile, paper, and plastic. The industries have grown rapidly in recent years and introduced dyes in our environment as wastes. Therefore, pollution of environment by them has become a critical problem for human health [1–20]. Removal of dyes from wastewater can occur by many methods such as adsorption, chemical oxidation, ion exchange, catalytic degradation, and biodegradation. Among these methods, adsorption is the most favorable because it is a simple, low cost, and effective method. So far, variety of adsorbents is investigated in adsorption procedure [2]. Graphene, a few layer of two-dimensional honeycomb arrange of sp^2 carbon atoms, has many unique properties such as great surface area and flat surface that convert it to a suitable adsorbent [7,13], but graphene has a hydrophobic surface; thus, it does not allow to disperse in water. The graphene oxide (GO) has all properties of graphene except it has a hydrophilic surface because it has a distribution of oxygenated functional group on its surface such as epoxide, carboxyl, and carbonyl group [20]. In addition, the GO can obtain in large quantity in a cheap procedure [15].

A literature review showed that the GO was applied to remove cationic dyes from binary systems.

*Corresponding author.

In this paper, the GO was prepared from graphite and it was used to remove cationic dyes from binary systems of colored wastewater. Basic blue 41 (BB41), basic red 18 (BR18), and basic red 46 (BR46) were used as model dyes. The prepared GO was characterized using Fourier transform infrared (FTIR), scanning electron microscopy (SEM), and X-ray diffraction (XRD). Kinetics and isotherm of dye adsorption were investigated in these systems.

2. Experimental

2.1. Materials and methods

Basic blue 41, basic red 18, and basic red 46 were used as model dyes. The chemical structure of dyes is shown in Fig. 1. Graphite, sulfuric acid 98%, potassium permanganate, sodium nitrite, hydrogen peroxide 30%, and hydrochloric acid 37% were purchased from Merck. All the materials were used without further purification.

2.2. Preparation of GO

GO was prepared by a modified Hummer method. Five hundred milliliter flask containing 2 g graphite powder was put in an ice bath (0˚C). A mixture of 100 mL H_2SO_4 98% and 4 g $NaNO_3$ was added to it with rigorous stirring. Ten gram $KMnO_4$ was added slowly to it, and then the reaction mixture was stirred for 48 h in room temperature. The resulting solution was viscose and brown color. Hundred milliliter deionized water was added to the resultant and was stirred for 1 h. Then, 20 mL H_2O_2 30% was added slowly by stirring the mixture. With the addition of hydrogen peroxide, the solution started bubbling and its color became yellow. The solid product was separated by centrifugation, and washed several times with 5% HCl solution and then with deionized water. Residue was dried in an air oven at 60˚C for 24 h. The graphite oxide was dispersed in water and exfoliated to GO nanosheet by probe ultrasonication for 1 h.

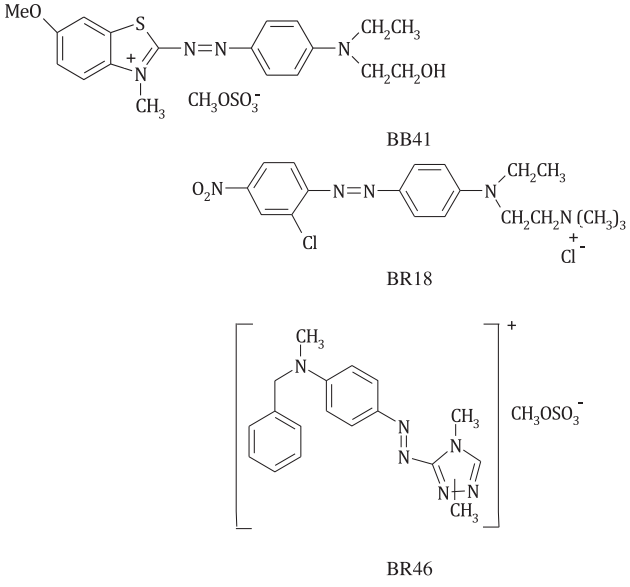

Fig. 1. The chemical structure of dyes.

The morphological structure of GO was examined by SEM (LEO 1455VP scanning microscope). The functional groups of GO were characterized by FTIR (Perkin-Elmer spectrophotometer spectrum one) in the range 4500–400 cm^{-1}. The crystallization behavior was identified by XRD model Siemens D-5000 diffractometer with Cu K_α radiation at room temperature.

2.3. Adsorption procedure

Dye adsorption is carried out by mixing 250 mL of dye solutions (50 mg/L) with adsorbent in jars, with a speed of 200 rpm at 25˚C for 60 min. In a certain interval of process time, absorbance of solutions was measured for determination of changes. At the end of dye adsorption process, solutions were centrifuged and their absorbance was determined. Maximum wavelength for measurement of absorbance of BR 18, BR 46, and BB41 were 488, 531, and 580 nm, respectively. The effect of adsorbent dosage and initial dye concentration on dye removal in single and binary systems was investigated.

Dye concentrations were calculated as follows. For a binary system, components A and B were measured at λ_1 and λ_2, respectively, to give optical densities of d_1 and d_2 [21]:

$$C_A = (k_{B2}d_1 - k_{B1}d_2)/(k_{A1}k_{B2} - k_{A2}k_{B1}) \quad (1)$$

$$C_B = (k_{A1}d_2 - k_{A2}d_1)/(k_{A1}k_{B2} - k_{A2}k_{B1}) \quad (2)$$

where k_{A1}, k_{B1}, k_{A2}, and k_{B2} are the calibration constants for components A and B at the two wavelengths λ_1 and λ_2, respectively.

3. Result and discussion

3.1. Characterization

The FTIR spectrum of graphite and GO is shown in Fig. 2. The FTIR spectrum of GO showed major stretching vibrations at 3,360, 1,729, 1,620, 1,222, and 1,051 cm^{-1} that are assigned to OH stretching (surface

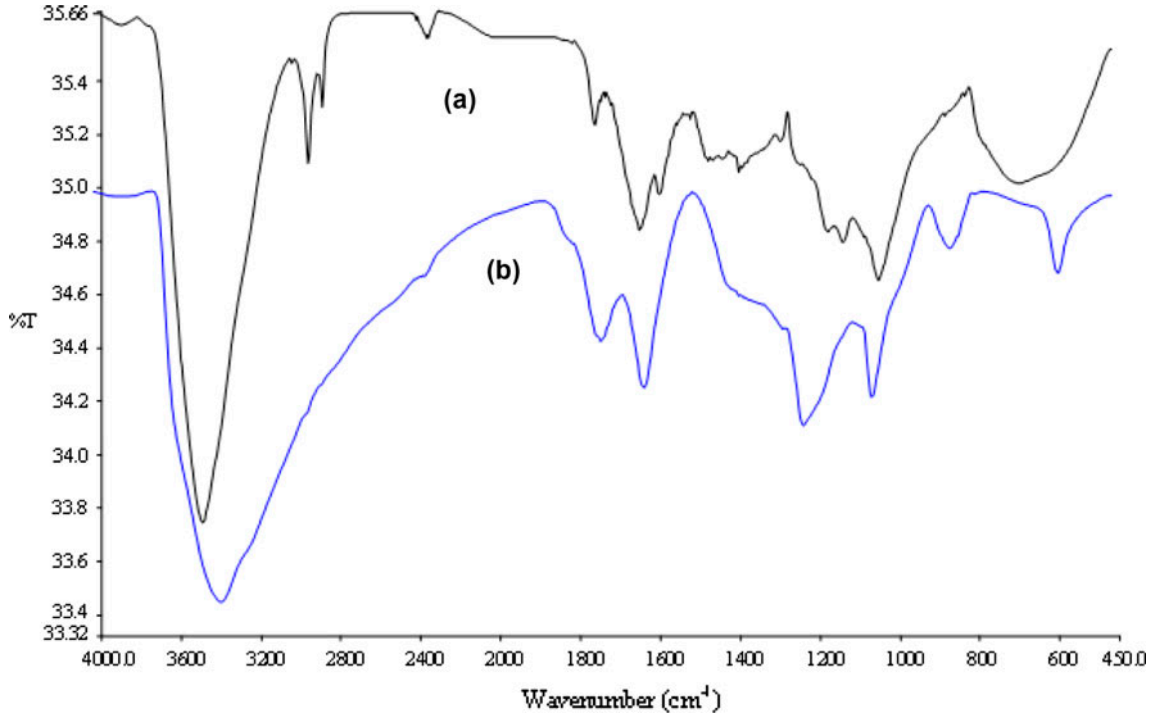

Fig. 2. FTIR spectra of samples (a) Graphite and (b) GO.

OH groups and absorbed water), –C=O stretching (COOH group), C=C stretching (aromatic rings), C–O stretching (COOH group), and C–O–C stretching (epoxy group), respectively [5,7,10,13,22].

The morphology of graphite and GO is investigated by SEM (Fig. 3). SEM is used to characterize the surface morphology and fundamental physical properties of material surface. The SEM image of GO nanosheet showed the layered structure.

Fig. 4 illustrates the XRD pattern of the graphite and GO. In XRD patterns of graphite and GO, the sharp diffraction peak at $2\theta = 26.52$ ($d = 0.336$ nm) corresponding to the normal graphite spacing (0 0 2) of the graphite plane disappeared in the XRD pattern of GO during oxidation process. The broad and relatively weak diffraction peak at $2\theta = 10.77$ ($d = 0.821$ nm) corresponding to the typical diffraction peak of GO is attributed to the (0 0 2) plane. This increased d-spacing

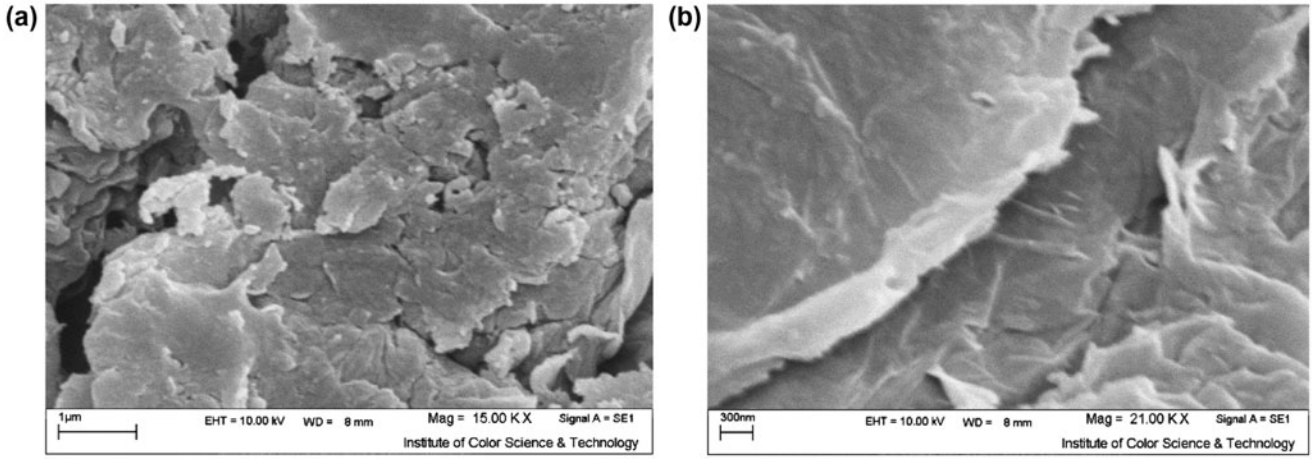

Fig. 3. SEM image of samples (a) Graphite and (b) GO.

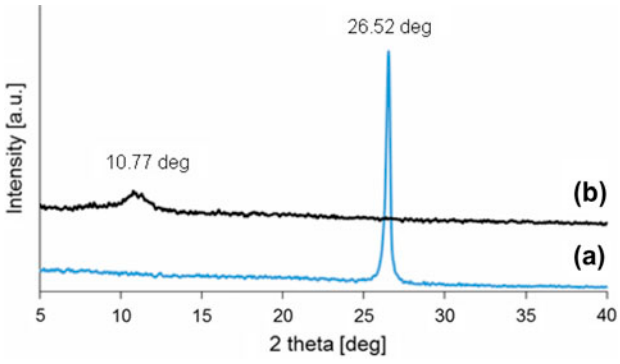

Fig. 4. XRD pattern of (a) Graphite and (b) GO.

from 0.336 to 0.821 nm is due to the creation of the abundant oxygen-containing functional groups on the surfaces of GO [23,24].

3.2. Adsorption kinetics

The mechanism of adsorption process is investigated by kinetics studies. The characteristic constants of adsorption kinetics were determined using pseudo-first order, pseudo-second order, and intraparticle diffusion models [25–27].

A linear form of pseudo-first-order model is:

$$\log(q_e - q_t) = \log(q_e) - (k_1/2.303)t \quad (3)$$

where q_e, q_t, and k_1 are the adsorbed dye on adsorbent at equilibrium (mg/g), the amount of adsorbed dye on adsorbent at time t (mg/g), and the equilibrium rate constant of pseudo-first-order kinetics (1/min), respectively.

To understand the applicability of the pseudo-first order for dye adsorption on GO at different amount of adsorbent, linear plots of log $(q_e - q_t)$ vs. contact time (t) are plotted (Fig. 5). The values of k_1, R^2, and the calculated q_e ($(q_e)_{cal}$) are shown in Table 1.

Linear form of pseudo-second-order model is shown as:

$$t/q_t = 1/k_2 q_e^2 + t/q_e \quad (4)$$

where k_2 is the equilibrium rate constant pseudo-second order (g/mg min).

To understand the applicability of the pseudo-second order for dye adsorption onto GO at different amount of adsorbent, linear plots of t/q_t vs. contact time (t) are plotted (Fig. 6). The values of k_2, R^2, and $(q_e)_{cal}$ are shown in Table 1.

The possibility of intraparticle diffusion resistance affecting adsorption is illustrated as:

$$q_t = k_p t^{1/2} + I \quad (5)$$

where k_p and I are constant intraparticle diffusion rate constant and intercept, respectively.

To understand the applicability of the intraparticle diffusion for dye adsorption onto GO at different amount of adsorbent, linear plots of q_t vs. $t^{1/2}$ are plotted (Fig. 7). The values of k_p, R^2, and I are shown in Table 1.

Linearity of plots shows that pseudo-first order and intraparticle diffusion does not play a significant role in kinetics of dye adsorption on GO in single and binary systems. The linear fit between the t/q_t vs. contact time (t) for pseudo-second-order kinetics model shows that the dye removal kinetic can be approximate as pseudo-second-order kinetics in both systems. In addition, the experimental q_e ($(q_e)_{Exp}$) values agree with the calculated ones ($(q_e)_{Cal.}$) obtained from the linear plots of pseudo-second-order kinetics.

3.3. Adsorption isotherm

The adsorption isotherm investigates the relation between mass of the adsorbed dye on to adsorbent and the temperature, particle size, and liquid phase of the dye concentration. Several isotherms such as Langmuir, Tempkin, and Freundlich models were studied in detail [25–27]. Langmuir isotherm assumes that adsorption takes place at specific sites within the adsorbent and is explained by the following equation:

$$C_e/q_e = 1/K_L Q_0 + C_e/Q_0 \quad (6)$$

where C_e, K_L, and Q_0 are equilibrium concentration of dye solution (mg/L), Langmuir constant, and maximum adsorption capacity (mg/g), respectively.

Isotherm data tested with Freundlich isotherm can be expressed by:

$$\log q_e = \log K_F + (1/n)\log C_e \quad (7)$$

where K_F is adsorption capacity at unit concentration and $1/n$ is adsorption intensity.

The Tempkin isotherm assumes that the heat of adsorption of all the molecules in the layer decreases linearly with coverage, and also the adsorption is characterized by a uniform distribution of binding energies up to some maximum binding energy, and is given by:

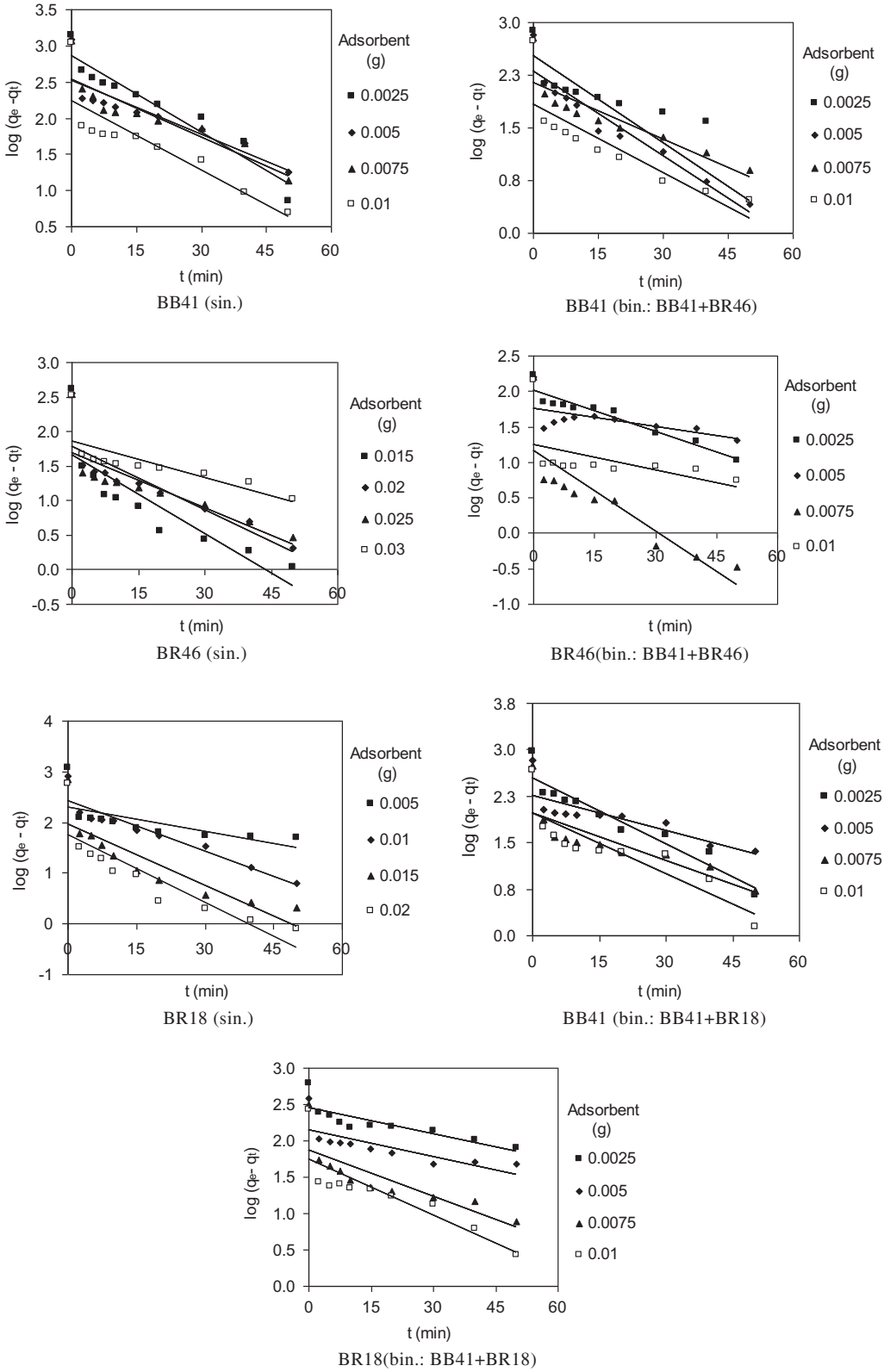

Fig. 5. Pseudo-first-order kinetics of dye removal by GO from single (sin.) and binary (bin.) systems.

Table 1
Linearized kinetics coefficients of dye removal using GO at different adsorbent dosages from single and binary systems

	Dye		Adsorbent (g/L)	$(q_e)_{Exp}$	Pseudo-first order			Pseudo-second order			Intraparticle diffusion		
					$(q_e)_{Cal.}$	k_1	R^2	$(q_e)_{Cal.}$	k_2	R^2	k_p	I	R^2
Single system	BB41		0.01	1413.67	736.21	0.0806	0.919	1428.57	0.0003	0.9988	71.9583	902.0370	0.9603
			0.02	1207.66	336.51	0.0553	0.787	1219.51	0.0006	0.9991	31.3964	964.9566	0.9959
			0.03	1193.68	349.14	0.0599	0.799	1204.82	0.0006	0.9992	35.3819	931.6300	0.9084
			0.04	1108.73	174.18	0.0714	0.746	1111.11	0.0016	0.9999	12.9284	1011.74	0.9836
	BR46		0.06	419.40	45.52	0.0868	0.7322	416.67	0.0082	1.0000	4.2388	391.05	0.7648
			0.08	361.05	62.34	0.0705	0.7586	357.14	0.0046	0.9999	5.2384	322.71	0.9739
			0.10	341.37	50.08	0.0608	0.6649	344.83	0.0053	0.9998	4.0398	310.31	0.9969
			0.12	337.35	72.54	0.0398	0.5659	333.33	0.0026	0.9985	6.3241	282.37	0.9504
	BR18		0.02	1201.52	201.79	0.0368	0.4517	1250.00	0.0011	0.9990	17.6590	1,047	0.9161
			0.04	806.09	264.61	0.0760	0.8964	833.33	0.0008	0.9996	25.3927	625	0.96
			0.06	698.25	94.95	0.0933	0.7796	714.29	0.0039	1.0000	9.4922	635.68	0.7755
			0.08	589.54	56.42	0.1013	0.7643	588.24	0.0072	1.0000	4.7357	558.29	0.7942
Binary system	BB41+BR18	BB41	0.01	953.47	359.17	0.0818	0.9061	1000.00	0.0006	0.9996	34.7590	709.1970	0.9333
			0.02	686.48	187.46	0.0440	0.6712	666.67	0.0010	0.9975	16.7743	543.6534	0.9152
			0.03	544.81	96.12	0.0590	0.6754	555.56	0.0025	0.9997	9.1136	476.8324	0.8222
			0.04	467.21	95.76	0.0751	0.755	476.19	0.0029	0.9996	7.6809	410.3373	0.8908
		BR18	0.01	615.40	285.96	0.0274	0.6979	588.24	0.0004	0.9812	31.6732	329.9235	0.8992
			0.02	379.66	140.51	0.0276	0.5912	370.37	0.0011	0.9897	14.6602	246.0263	0.9094
			0.03	320.15	73.89	0.0486	0.6694	322.58	0.0029	0.9992	7.6653	260.9981	0.9271
			0.04	268.08	56.21	0.0590	0.7175	270.27	0.0039	0.9994	4.5442	231.9391	0.9665
	BB41+BR46	BB41	0.01	773.32	339.55	0.0953	0.7237	769.23	0.0008	0.9984	22.0223	604.3633	0.9851
			0.02	660.77	204.17	0.0924	0.9150	666.67	0.0013	0.9999	21.0887	519.6639	0.8407
			0.03	598.54	139.19	0.0615	0.7747	588.24	0.0018	0.9997	13.9769	496.3377	0.9404
			0.04	538.26	70.50	0.0746	0.7200	526.32	0.0052	1.0000	6.0642	495.4125	0.9266
		BR46	0.01	170.01	103.01	0.0440	0.9115	178.57	0.0010	0.9832	11.9337	74.1425	0.9561
			0.02	160.98	57.39	0.0196	0.3794	153.85	0.0020	0.9785	4.4326	109.2943	0.4928
			0.03	158.55	14.76	0.0873	0.7180	158.73	0.0248	1.0000	1.0169	151.3264	0.9491
			0.04	144.51	18.09	0.0274	0.2556	142.86	0.0114	0.9987	1.0597	132.2227	0.5992

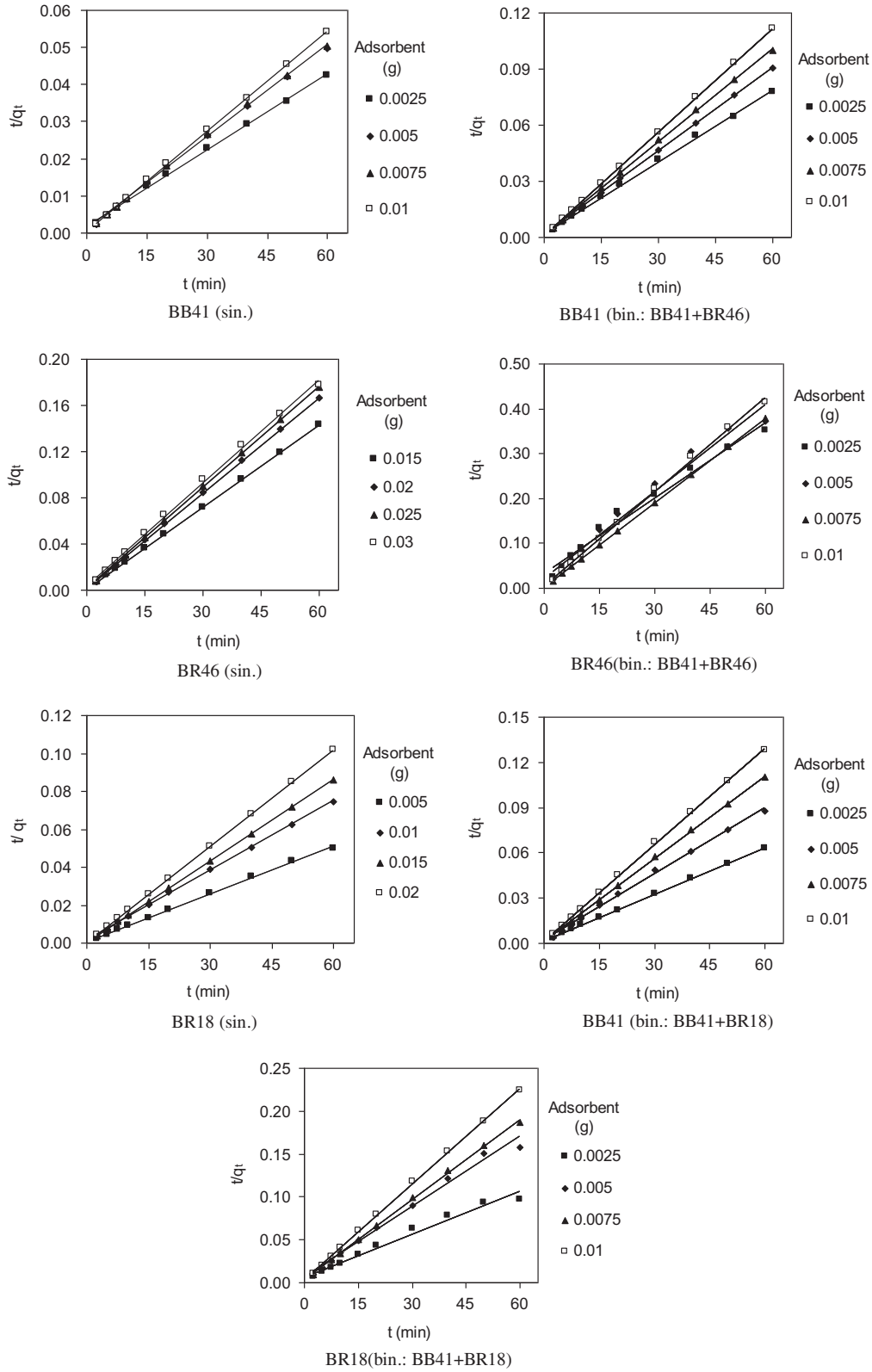

Fig. 6. Pseudo-second-order kinetics of dye removal by GO from single (sin.) and binary (bin.) systems.

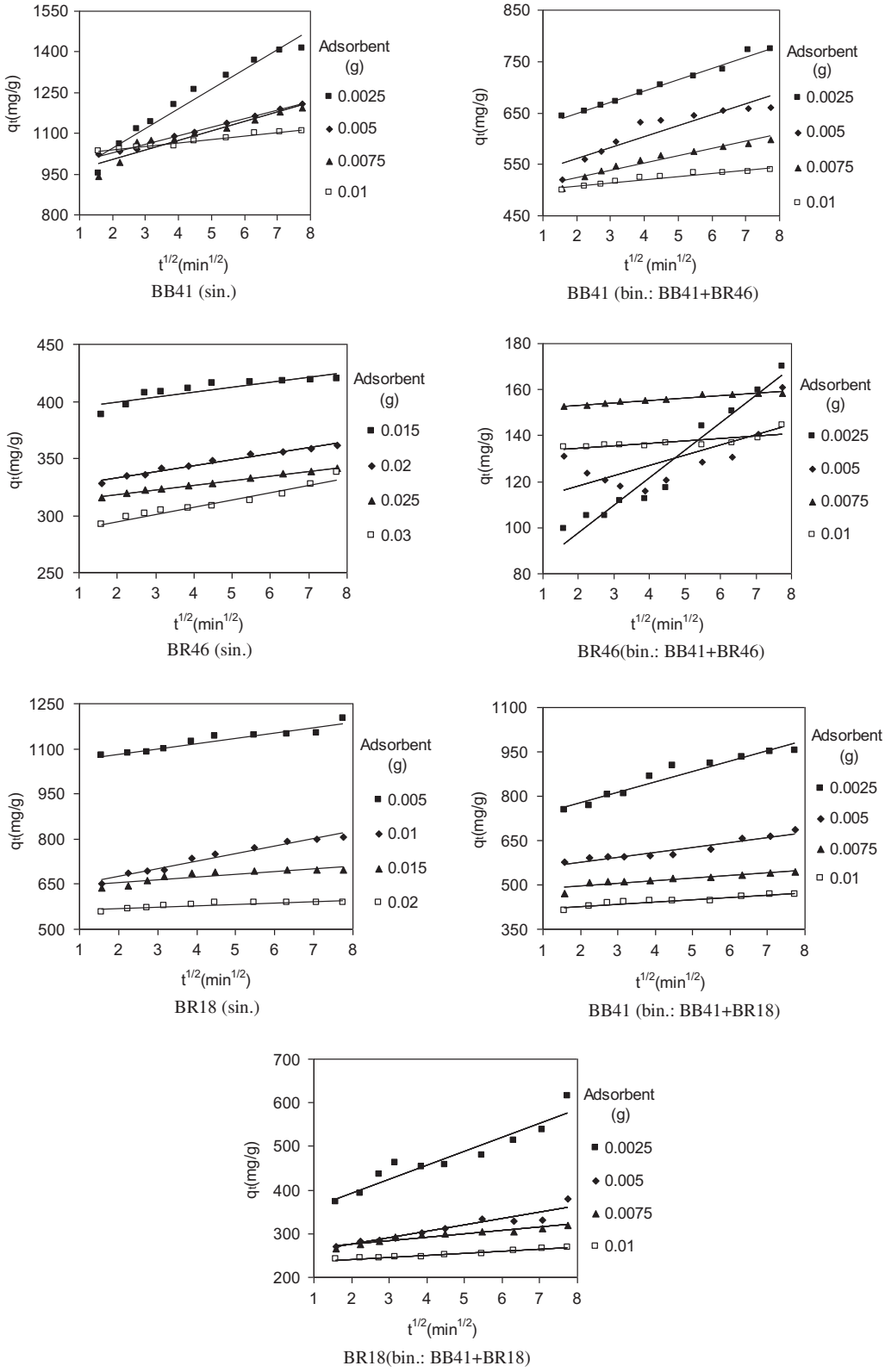

Fig. 7. Intraparticle diffusion kinetics of dye removal by GO from single (sin.) and binary (bin.) systems.

Table 2
Linearized isotherm coefficients of dye removal using GO at different adsorbent dosages from single and binary systems

System		Langmuir			Freundlich			Tempkin		
		Q_0	K_L	R^2	K_F	$1/n$	R^2	K_T	B_1	R^2
Single system		BB41								
		1,429	0.3684	**0.9805**	902.82	0.1091	**0.7508**	135.66	528.0	**0.7234**
		BR18								
		1,250	0.1702	**0.8687**	414.57	0.2808	**0.8171**	233.99	3.0	**0.7359**
		BR46								
		476	0.2019	**0.9409**	213.25	0.1890	**0.6319**	70.45	10.0	**0.6136**
Binary system	BB41+BR18	BB41								
		1,639	0.0858	**0.9710**	204.31	0.5558	**0.9940**	379.37	0.7	**0.9745**
		BR18								
		417	0.0330	**0.9089**	1.9320	1.9813	**0.9787**	844.21	0.1	**0.9654**
	BB41+BR46	BB41								
		870	0.3795	**0.9826**	407.85	0.2168	**0.9431**	139.20	14.0	**0.9148**
		BR46								
		625	0.0156	**0.0938**	14.5512	0.7765	**0.4927**	118.65	0.2	**0.4708**

$$q_e = B_1 \ln K_T + B_1 \ln C_e \quad (8)$$

where $B_1 = RT/b$, K_T is the equilibrium binding constant (L/mol) corresponding to the maximum binding energy, and B_1 is related to the heat of adsorption. Also, R and T are the gas constant and the absolute temperature, respectively.

To study the applicability of the Langmuir, Tempkin, and Freundlich isotherms for dye adsorption onto GO from single and binary systems at different adsorbent dosage, linear plots of C_e/q_e against C_e, log q_e vs. log C_e, and q_e vs. ln C_e are plotted. The values of Q_0, K_L, K_F, $1/n$, K_T, B_1, and R^2 are shown in Table 2.

The R^2 values show that the dye removal isotherm using GO adsorbent for BB41, BR 18, and BR 46 in single systems follows the Langmuir, in binary system BB41 and BR 18 follows the Freundlich, and in binary system BB41 and BR 46 follows the Langmuir and

Table 3
Adsorption capacities of different GO adsorbents to remove dyes (rGO: reduced GO)

Adsorbent	Adsorbate	Q_0 (mg/g)	Reference
GO	Pyrene	96	[28]
rGO	Pyrene	198	
	Anthracene	81	
	Naphtalene	767	
GO–iron oxides, 303 K	Pb(II)	588	[29]
rGO–iron oxides, 303 K	Pb(II)	454	
GO–iron oxides, 303 K	1-naphthol	228	
rGO–iron oxides, 303 K	1-naphthol	243	
rGO–iron oxides, 323 K	1-naphthol	357	
rGO–iron oxides, 343 K	1-naphthol	588	
GO–iron oxides, 303 K	1-naphthylamine	286	
rGO–iron oxides, 303 K	1-naphthylamine	303	
rGO–iron oxides, 323 K	1-naphthylamine	400	
rGO–iron oxides, 343 K	1-naphthylamine	625	
Sulfonated GO	Naphthalene	307	[30]
	1-naphthol	346	
GO	BB 41	1,429	Present study
	BR 18	1,250	
	BR 46	476	

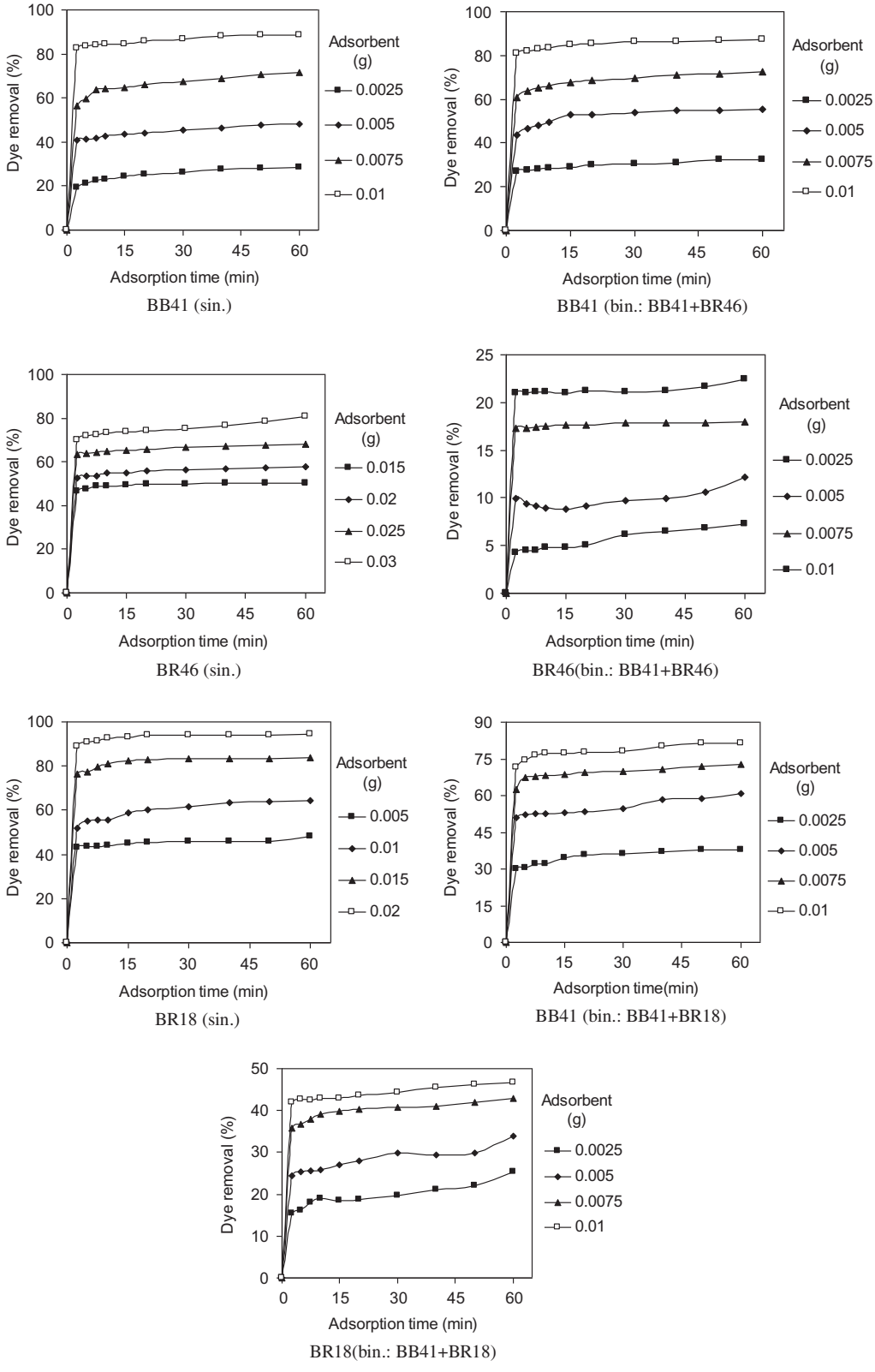

Fig. 8. The effect of adsorbent dosage on dye removal by GO from single (sin.) and binary (bin.) systems.

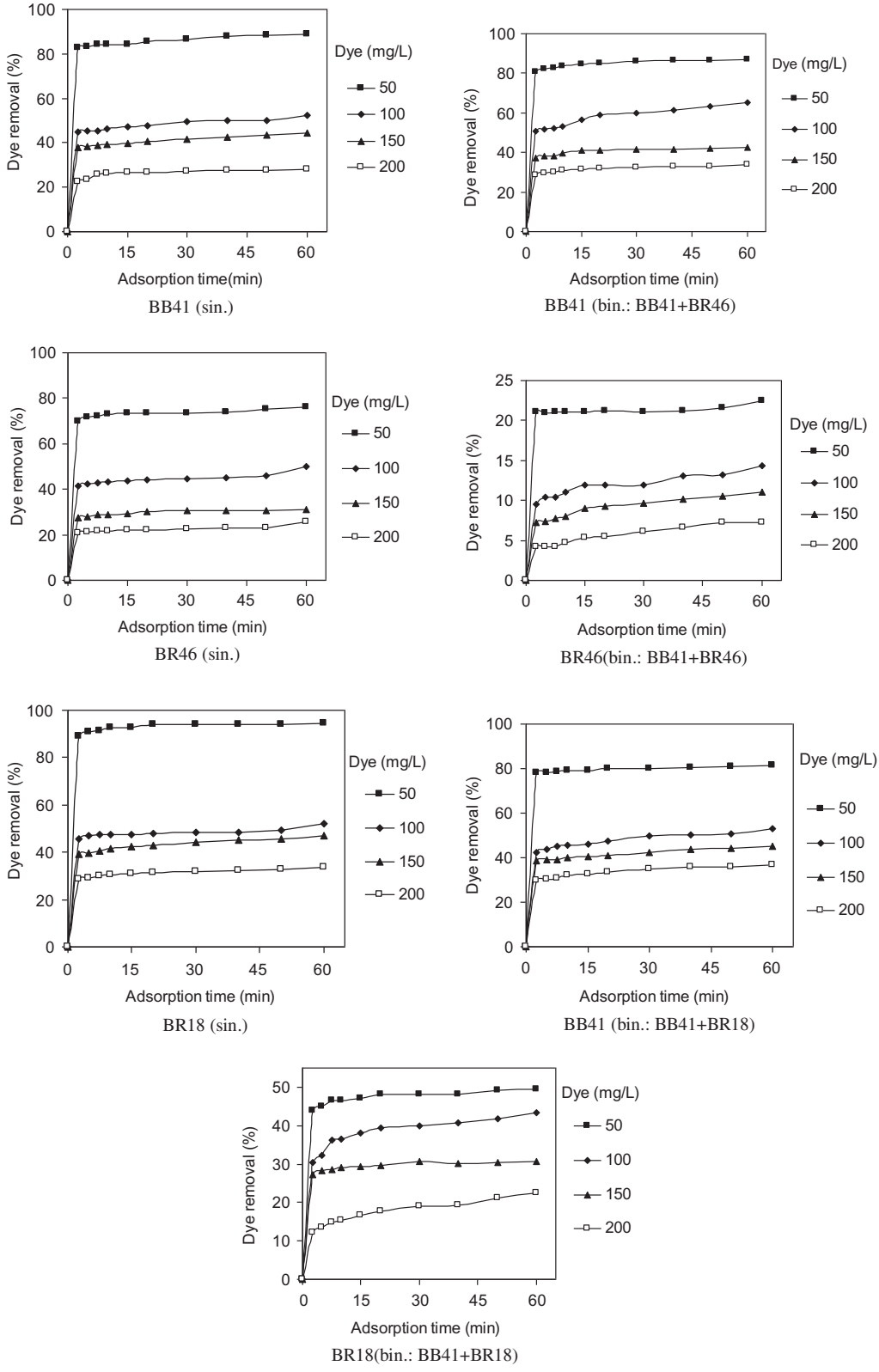

Fig. 9. The effect of dye concentration on dye removal by GO from single (sin.) and binary (bin.) systems.

Freundlich, respectively. The BR 18 and BB41 have linear structures, but BR 46 has a nonlinear structure. The structure of BR 46 makes a steric hindrance for adsorption. Therefore adsorption of BR 18 and BB 41 on GO are more than BR 46.

The maximum adsorption capacity (Q_0) of several adsorbents is shown in Table 3. The results show that the prepared GO has high dye adsorption capability. Thus, it can be used as a high-capacity adsorbent to remove cationic dyes.

3.4. Effect of operational parameter on dye removal

3.4.1. Effect of adsorbent dosage

The percentage of dye removal from single and binary systems vs. time (min) at different GO dosages from single and binary systems is shown in Fig. 8. Dye removal increases when GO dosage increases (dye removal of 0.0025, 0.005, 0.0075, and 0.01 g GO was 28, 48, 72, and 89%, respectively, for BB41; dye removal of 0.005, 0.01, 0.015, and 0.02 g GO was 48, 64, 84, and 94%, respectively, for BR 18; dye removal of 0.015, 0.02, 0.025, and 0.03 g GO was 50, 58, 68, and 81%, respectively, for BR 46). The increase in dye removal with adsorbent dosage can be attributed to increased adsorbent surface and availability of more adsorption sites.

3.4.2. Effect of dye concentration

The dye removal (%) from single and binary systems vs. time (min) at different dye concentration (mg/L) is shown in Fig. 9. Dye removal of GO at 50, 100, 150, and 200 mg/L dye concentration was 89, 52, 44, and 28% for BB 41 dye, and 94, 52, 46, and 33% for BR 18 dye, and 76, 50, 31, and 25% for BR 46, respectively. The amount of the dye absorbed onto GO increases with an increase in the initial dye concentration of solution.

4. Conclusion

In this paper, the GO was prepared and used as an adsorbent to remove three cationic dyes (BB 41, BR 18, and BR 46) from single and binary systems. The GO was characterized using FTIR, SEM, and XRD. There is an electrostatic interaction between the negatively charged groups in the GO and the cationic dye molecules. The adsorption of BR 18 and BB 41 on GO are more than BR 46. The BR 18 and BB41 have linear structures, but BR 46 has a nonlinear structure. The structure of BR 46 makes a steric hindrance for adsorption. Dye removal increases with the adsorbent dosage. It was found that adsorption kinetic of dyes in both systems follow with pseudo-second-order kinetics. Also, results showed that adsorption of three dyes in both systems conform to Langmuir isotherm. The maximum dye adsorption capacity of GO for BB 41, BR 18, and BR 46 were 1,429, 1,250, and 476 mg/g, respectively, that are high dye adsorption capacities. Therefore, GO can be a suitable adsorbent to remove cationic dyes from wastewater.

Acknowledgment

This work was done in the Department of Environmental Research, Institute for Color Science and Technology. Professor Mahmoodi is grateful for the support from the ICST.

References

[1] T. Kuila, S. Bose, A.K. Mishra, P. Khanra, N.H. Kim, J.H. Lee, Chemical functionalization of graphene and its applications, Prog. Mater. Sci. 57 (2012) 1061–1105.
[2] Q. Wu, Ch Feng, Ch Wang, Z. Wang, A facile one-pot solvothermal method to produce superparamagnetic graphene-Fe_3O_4 nanocomposite and its application in the removal of dye from aqueous solution, Colloids Surf. B 101 (2013) 210–214.
[3] G.K. Ramesha, A. Vijaya Kumara, H.B. Muralidhara, S. Sampath, Graphene and graphene oxide as effective adsorbents toward anionic and cationic dyes, J. Colloid Interface Sci. 361 (2011) 270–277.
[4] G. Xie, P. Xi, H. Liu, F. Chen, L. Huang, Y. Shi, F. Hou, Zh Zeng, Ch Shao, J. Wang, A facile chemical method to produce superparamagnetic graphene oxide–Fe_3O_4 hybrid composite and its application in the removal of dyes from aqueous solution, J. Mater. Chem. 22 (2012) 1033–1039.
[5] Y. Li, Q. Du, T. Liu, X. Peng, J. Wang, J. Sun, Y. Wang, Sh Wu, Z. Wang, Y. Xia, L. Xia, Comparative study of methylene blue dye adsorption onto activated carbon, graphene oxide, and carbon nanotubes, Chem. Eng. Res. Des. 91 (2013) 361–368.
[6] S. Bai, X. Shen, X. Zhong, Y. Liu, G. Zhu, X. Xu, K. Chen, One-pot solvothermal preparation of magnetic reduced graphene oxide-ferrite hybrids for organic dye removal, Carbon 50 (2012) 2337–2346.
[7] P. Sharma, M.R. Das, Removal of a cationic dye from aqueous solution using graphene oxide nanosheets: Investigation of adsorption parameters, J. Chem. Eng. Data 58 (2013) 151–158.
[8] F. Liu, S. Chung, G. Oh, T.S. Seo, Three-dimensional graphene oxide nanostructure for fast and efficient water-soluble dye removal, Appl. Mater. Interfaces 4 (2012) 922–927.
[9] L. Kui, Z. Guixia, W. Xiangke, A brief review of graphene-based material synthesis and its application in environmental pollution management, Chin. Sci. Bull. 57 (2012) 1223–1234.

[10] L. Fan, Ch Luo, M. Sun, H. Qiu, X. Li, Synthesis of magnetic β-cyclodextrine-chitosan/graphene oxide as nanoadsorbent and its application in dye adsorption and removal, Colloids Surf., B 103 (2013) 601–607.
[11] L. Meijiao, L. Jing, Y.X. Yu, Z. Chang, Y. Jia, H. Hao, W. Xianbao, Applications of graphene-based materials in environmental protection and detection, Chin. Sci. Bull. 58 (2013) 2698–2710.
[12] Seul-Yi Lee, Soo-Jin Park, Comprehensive review on synthesis and adsorption behaviors of graphene-based materials, Carbon Lett. 13 (2012) 73–87.
[13] H. Sun, L. Cao, L. Lu, Magnetite/reduced graphene oxide nanocomposites: One step solvothermal synthesis and use as a novel platform for removal of dye pollutants, Nano Res. 4 (2011) 550–562.
[14] S. Wang, Sh Lv, Zh Guo, F. Jiang, Removal of organic dyes in environmental water onto magnetic-sulfonic graphene nanocomposite, Clean Soil Air Water 41 (2013) 992–1001.
[15] L. Sun, H. Yu, B. Fugetsu, Graphene oxide adsorption enhanced by *in situ* reduction with sodium hydrosulfite to remove acridine orange from aqueous solution, J. Hazard. Mater. 203–204 (2012) 101–110.
[16] Ch Wang, Ch Feng, Y. Gao, X. Ma, Q. Wu, Zh Wang, Preparation of a graphene-based magnetic nanocomposite for the removal of an organic dye from aqueous solution, Chem. Eng. J. 173 (2011) 92–97.
[17] T. Wu, X. Cai, Sh Tan, H. Li, J. Liu, W. Yang, Adsorption characteristics of acrylonitrile, p-toluenesulfonic acid, 1-naphthalenesulfonic acid and methyl blue on graphene in aqueous solutions, Chem. Eng. J. 173 (2011) 144–149.
[18] L. Ai, J. Jiang, Removal of methylene blue from aqueous solution with self-assembled cylindrical graphene-carbon nanotube hybrid, Chem. Eng. J. 192 (2011) 156–163.
[19] B. Wang, B. Luo, M. Liang, A. Wang, J. Wang, Y. Fang, Y. Chang, L. Zhi, Chemical amination of graphene oxides and their extraordinary properties in the detection of lead ions, Nanoscale 3 (2011) 5059–5066.
[20] Y. Gao, Y. Li, L. Zhang, H. Huang, J. Hu, S.M. Shah, X. Su, Adsorption and removal of tetracycline antibiotics from aqueous solution by graphene oxide, J. Colloid Interface Sci. 368 (2012) 540–546.
[21] K.K.H. Choy, J.F. Porter, G. McKay, Langmuir isotherm models applied to the multicomponent sorption of acid dyes from effluent onto activated carbon, J. Chem. Eng. Data. 45 (2000) 575–584.
[22] A.M. Shanmugharaj, J.H. Yoon, W.J. Yang, Synthesis, characterization, and surface wettability properties of amine functionalized graphene oxide films with varying amine chain lengths, J. Colloid Interface Sci. 401 (2013) 148–154.
[23] George Z. Kyzas, Nikolina A. Travlou, Orestis Kalogirou, Eleni A. Deliyanni, Magnetic graphene oxide: Effect of preparation route on Reactive Black 5 adsorption, Materials 6 (2013) 1360–1376.
[24] Soumen Dutta, Sougata Sarkar, Chaiti Ray, Tarasankar Pal, Benzoin derived reduced graphene oxide (rGO) and its nanocomposite: Application in dye removal and peroxidase-like activity, RSC Adv. 3 (2013) 21475–21483.
[25] N.M. Mahmoodi, Magnetic ferrite nanoparticle–alginate composite: Synthesis, characterization and binary system dye removal, J. Taiwan Inst. Chem. Eng. 44 (2013) 321–329.
[26] N.M. Mahmoodi, Synthesis of amine-functionalized magnetic ferrite nanoparticle and its dye removal ability, J. Environ. Eng. 139 (2013) 1382–1390.
[27] N.M. Mahmoodi, Dendrimer functionalized nanoarchitecture: Synthesis and binary system dye removal, J. Taiwan Inst. Chem. Eng. 45 (2014) 2008–2020.
[28] Yubing Sun, Shubin Yang, Guixia Zhao, Qi Wang, Xiangke Wang, Adsorption of polycyclic aromatic hydrocarbons on graphene oxides and reduced graphene oxides, Chem. Asian J. 8 (2013) 2755–2761.
[29] Xin Yang, Changlun Chen, Jiaxing Li, Guixia Zhao, Xuemei Ren, Xiangke Wang, Graphene oxide-iron oxide and reduced graphene oxide-iron oxide hybrid materials for the removal of organic and inorganic pollutants, RSC Adv. 2 (2012) 8821–8826.
[30] Guixia Zhao, Lang Jiang, Yudong He, Jiaxing Li, Huanli Dong, Xiangke Wang, W. Hu, Sulfonated graphene for persistent aromatic pollutant management, Adv. Mater. 23 (2011) 3959–3963.